

## Article

# Multiscale Structural Analysis of Ediacaran–Cambrian Rocks on the Northeastern Edge of the Saghro Inlier (Eastern Anti-Atlas): Relevance of Post-Cambrian Deformation

Zakarya Yajoui <sup>1</sup>, Helena Sant’Ovaia <sup>2,\*</sup> , Brahim Karaoui <sup>1</sup> , Cláudia Cruz <sup>2</sup> , Amar Karaoui <sup>3</sup>, Abdelkader Mahmoudi <sup>3</sup>, Hmidou El Ouardi <sup>3</sup> and Lakhlifi Badra <sup>3</sup>

<sup>1</sup> Applied Geology Laboratory, Faculty of Sciences and Techniques, Moulay Ismail University of Meknes, Boutalamine, Errachidia P.O. Box 509, Morocco; yajoui91@gmail.com (Z.Y.); karaouibrahim@yahoo.fr (B.K.)

<sup>2</sup> Instituto de Ciências da Terra—Polo da Universidade do Porto, Departamento de Geociências, Ambiente e Ordenamento do Território, Faculdade de Ciências, Universidade do Porto, Rua do Campo Alegre s/n, 4169-007 Porto, Portugal; claudiacruz@fc.up.pt

<sup>3</sup> Faculty of Sciences, Moulay Ismail University of Meknes, Zitoune, Meknes P.O. Box 11201, Morocco; amar.karaoui@yahoo.com (A.K.); geo\_mahmoudi@yahoo.fr (A.M.); h.elouardi@fs-umi.ac.ma (H.E.O.); badra\_lakhlifi@yahoo.fr (L.B.)

\* Correspondence: hsantov@fc.up.pt

**Abstract:** The Ediacaran–Cambrian rocks on the northeastern edge of the Saghro inlier experienced polycyclic tectono-thermal events, which are reported here based on a multiscale structural analysis, from field measurements to fluid inclusion planes. Three striking populations were identified, cutting across both the Ediacaran and Cambrian formations. These tectonic structures were generated during four tectonic events. (i) E–W-striking structures that host ore mineralized bodies (sulfide, oxide, quartz, and barite). They display a polyphase tectonic history, caused by a dextral movement in response to a NW–SE-oriented shortening, leading to the formation of quartz gashes and veins. This tectonic event took place during the Neovariscan. These E–W-striking structures were subsequently reactivated during the Mesozoic time under a sinistral strike-slip regime as a result of NE–SW shortening synkinematic with barite mineralization. (ii) NE–SW-striking strike-slip structures (dextral or sinistral) crosscut the E–W-striking veins. These faults are related to the NW–SE-oriented shortening that occurred during the Neogene. (iii) The last tectonic episode, related to the N–S shortening, took place during the late Neogene to the Quaternary period. It resulted in NW–SE to N–S-striking structures that were related to dextral and sinistral strike-slip movements, which crosscut the preexisting E–W structures.

**Keywords:** multiscale analysis; post-Cambrian tectonism; Saghro inlier; Precambrian



**Citation:** Yajoui, Z.; Sant’Ovaia, H.; Karaoui, B.; Cruz, C.; Karaoui, A.; Mahmoudi, A.; El Ouardi, H.; Badra, L. Multiscale Structural Analysis of Ediacaran–Cambrian Rocks on the Northeastern Edge of the Saghro Inlier (Eastern Anti-Atlas): Relevance of Post-Cambrian Deformation.

*Geosciences* **2023**, *13*, 258. <https://doi.org/10.3390/geosciences13090258>

Academic Editors: Olivier Lacombe and Jesus Martinez-Frias

Received: 29 May 2023

Revised: 10 August 2023

Accepted: 15 August 2023

Published: 24 August 2023



**Copyright:** © 2023 by the authors. Licensee MDPI, Basel, Switzerland. This article is an open access article distributed under the terms and conditions of the Creative Commons Attribution (CC BY) license (<https://creativecommons.org/licenses/by/4.0/>).

## 1. Introduction

Structural analysis plays a pivotal role in understanding the complex geological history that has been recorded in an area since it offers valuable information on the Earth’s geodynamic evolution. It includes interpreting and examining various tectonic structures, such as faults, folds, fractures, and rock fabrics. This analysis can be conducted on different scales ranging from satellite imagery to microscopic analysis. Also, it enables the determination of orientation, geometry, and distribution, as well as the spatial relationships between different tectonic structures. Such information can be used to reconstruct the geological evolution of the region, thus determining the timing of different tectonic events recorded in the region. These pieces of information are practically significant for mining exploration, as they provide valuable insights into both mineralized and unmineralized tectonic events.

On the northern edge of the West African Craton, the Anti-Atlas belt has experienced various tectonic events from the Proterozoic to the Phanerozoic times. In this belt,

the Precambrian basement crops out within several inliers beneath the Paleozoic cover (Figure 1A), such as Bas Draâ, Ifni, Kerdous, Tagragra of Akka, Agadir Melloul-Iguerda, Igherm, Zenaga, Siroua, Bou Azzer, Saghro, and Ougnat [1–3]. Two Precambrian orogenic cycles have been recognized in the Anti-Atlas belt: (i) the Eburnean orogeny during the Paleoproterozoic, and (ii) the Pan-African orogeny that spanned the Neoproterozoic. Later, during the Phanerozoic, the inherited Precambrian tectonic structures played a major role in the tectono-sedimentary evolution of the Anti-Atlas [4,5]. During the collision of Laurasia with Gondwana, the Paleozoic sedimentary successions in the Anti-Atlas basins were deformed and folded, whereas large blocks of its Precambrian basement were uplifted as inliers or “boutonniers” [4–6]. Due to the lack of Mesozoic–Cenozoic lithostratigraphic landmarks, post-Variscan deformation in the Anti-Atlas has been excluded so far, and therefore it has been considered pre-Alpine [7,8]. However, recent apatite and zircon fission-track data reveal fingerprints of Atlas-style tectonism and exhumation of the Precambrian belt during the Mesozoic–Cenozoic time [6,9–13].

The current paper is concerned with the use of different geological approaches applied in structural geology on different scales, from regional field analysis to fluid inclusion plane measurements, to highlight the post-Cambrian tectonic events that are recorded within the Ediacaran and Cambrian rocks on the NE edge of the Saghro inlier. Furthermore, the relationship between ore deposits and tectonism is discussed. The results are crucial on a regional scale and have implications for mining districts within the Saghro inlier and in the Anti-Atlas belt.

## 2. Geology of the NE Edge of the Saghro Inlier

The NE margin of the Saghro inlier (eastern Anti-Atlas) mainly consists of an Ediacaran basement and Paleozoic cover (Figure 1B). The basement comprises metasedimentary successions with subvolcanic sills and dykes of the Saghro Group, which crops out in several restricted areas, such as Imiter, Sidi Flah-Bouskour, Boumalne, and Kalaa M’Gouna [14]. These formations were regarded as Cryogenian based on lithofacies correlations and deformation styles [15,16]. Recently, U-Pb ages of detrital zircon grains from the Imiter and Boumalne inliers have indicated maximum depositional ages of  $607 \pm 6$  Ma and  $604 \pm 5$  Ma [17]. The Saghro Group is unconformably overlain by the Ediacaran Ouarzazate Supergroup. The latter consists of thick volcano-sedimentary successions and their plutonic equivalents [18–23]. The Ouarzazate Supergroup itself unconformably underlies Cambrian sedimentary sequences [14,19,20]. These Cambrian units are represented by monoclinal successions, dipping to the north. The Cambrian Series 2, representing the Lower Cambrian, begins with the Igoudine Formation comprising mainly polygenic conglomerates. The Igoudine Formation is overlain by the Issafène/Imouslek Formation composed of conglomerates and carbonates. The Asrir Formation consists mainly of quartzitic sandstone and forms the uppermost unit of the Lower Cambrian. The Cambrian Series 3, representing the Middle Cambrian formation, is composed of greenish schists of the Jbel Wawrmast Formation, showing interbedded lenses of carbonates and sandstone layers. The top is characterized by massive white quartzitic sandstones of the Jbel Afraou Formation [19,20].

The overprints of the Variscan to Alpine (Atlasic) orogenies have been reported by [9,24], respectively. During the Palaeozoic, two tectonic phases have been documented (D1 and D2) within the Ouaklim and Tilouine Palaeozoic allochthonous units [24]. These phases are related to the Neovariscan tectonism dated to 300–290 Ma and are equivalent to the oblique convergence between Gondwana and Laurussia which is also observed in the entire Moroccan Variscides [25]. The D1 phase corresponds to a thin-skinned tectonic style that led to nappe stacking and southward thrusting of allochthonous units, and generation of the diagenesis–anchizone transition to anchizone grade metamorphism. On the other hand, the D2 phase corresponds to a thick-skinned tectonic style that generated an E–W-striking fault system with a right-lateral offset.

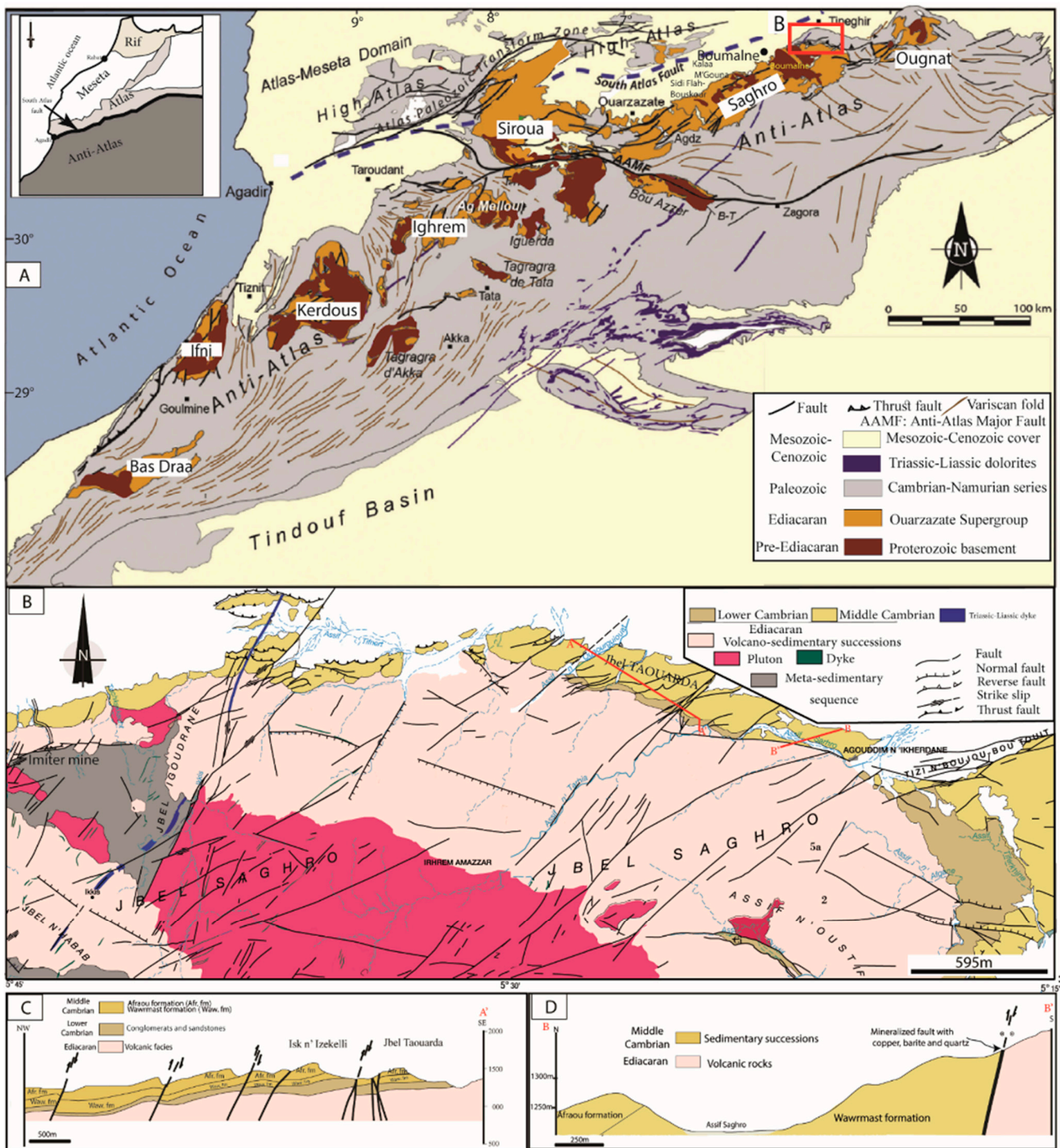


**Figure 1. (A)** Structural map of the Moroccan Anti-Atlas Mountains, after [26]. **(B)** Geological map of the northeastern Saghro inlier modified after [19,20]. **(C)** WNW-ESE cross-section showing NE-SW and N-S-oriented fault systems cutting Ediacaran and Cambrian formations [20]. **(D)** NE-SW cross-section illustrating fault contact between Ediacaran–Cambrian rocks; this fault shows a dextral strike-slip movement with a normal component.

Cerrina Feroni et al. [9] reported fission-track data indicating a post-Variscan evolution of the eastern Anti-Atlas. According to the same authors, four tectonic phases can be recognized: (i) D1 event, which occurred during the Mesozoic and corresponds to a left-lateral transtensional regime described along the Tizi n’Boujou and Bou Larhazail-Tinifift Faults; (ii) D2 event, which corresponds to a NW-SE-oriented shortening that took place during the Neogene. It was responsible for right-lateral transpressional tectonics documented along the Tizi n’Boujou and Isk n’Izekelli Faults; and (iii) D3 and D4 events,

which occurred during the Late Neogene and are still active. These are the result of NNE–SSW- to NNW–SSE-oriented regional shortening (D3 and D4, respectively), which induced remarkable fault reactivation, seismicity, and volcanism.

### 3. Materials and Methods

To identify the different tectonic events recorded within the Ediacaran and Cambrian rocks during the post-Cambrian time, a detailed tectonic analysis, ranging from regional mapping to microscopic observations, was carried out. It included geometric and kinematic measurements of fault planes (strike, dip-angle, and slickenline) of different regional faults. Moreover, measurements of vein and fracture networks in different rocks from the Ediacaran and Cambrian were complemented by data from fluid inclusion planes hosted in quartz and barite veins. The chronology between various tectonic structures was established by examining the presence or absence of the fault fillings, conducting tectoglyph analysis of different fault systems, and evaluating crosscutting relationships. The results are presented in stereograms (using lower hemisphere) with a Schmidt canvas using the Stereonet program.

Fluid inclusion planes (FIP) correspond to secondary fluid inclusions that developed after the growth of the crystals. They result from the healing of former open cracks and appear to be fossilized fluid pathways [27–29]. The fluid inclusion planes occur in sets and are formed as mode-I cracks materializing the  $\sigma_1$ – $\sigma_2$  plane [30]. They provide valuable information about local paleo-stress in rocks [27] and allow for establishing the relationships between tectonic events and fluid percolations.

FIP were measured in quartz and barite veins. The analyses were performed in oriented thin sections (related to the geographic north) using an image analyzer attached to a transmitted light microscope. Image acquisition, analysis, and mapping of the fluid inclusion planes were performed using the software GeoImagin (<https://home.uevora.pt/~pmn/geoimagin/index.html> accessed on 28 May 2023).

## 4. Results

### 4.1. Field Measurements

Several field campaigns and measurements have been conducted on different tectonic structures on the NE edge of the Saghro inlier. These measurements provided valuable insights into the presence of distinct orientations of faults. These orientations correspond to regional fault structures as well as mineralized veins or lenses. Notably, these structures cut the Ediacaran basement and continue into the Paleozoic cover (Figure 1C,D). Through the analysis of fault fillings and crosscutting relationships, three distinct tectonic structure populations have been recognized, which are an E–W-striking system, a NE–SW-striking system, and a NW–SE- to N–S-striking system (Figure 2A). The three identified populations of tectonic structures are described below.

#### 4.1.1. E–W-Striking Structures

E–W-striking structures represent the most prominent feature on the NE edge of the Saghro inlier. These tectonic structures predominantly appear as veins and faults. The rose diagram ( $N n = 250$ ) of the mineralized veins shows that the orientation is a well-defined E–W-striking system (Figure 2). These structures exhibit orientations ranging from  $N80^\circ$  to  $N120^\circ$ , dipping between  $55^\circ$  and  $90^\circ$  towards the south and occasionally to the north (Figures 1D and 2B,C). These mineralized structures appear to be controlled by strike-slip tectonic movements. Quartz and barite represent the main gangue filling of these veins. Based on the textural relationship between quartz and barite (Figure 2D,E) and the preserved microtectonic motion indicators within these structures (Figure 2), two superposed tectonic stages have been identified. The first one corresponds to a dextral strike-slip with a normal component (Figure 2B,C), which is syn-kinematic with the quartz veins (Figure 2F,G). These veins are the result of NW–SE shortening. The second stage evolved through sinistral movement with a normal component resulting from NE–SW shortening contemporaneous with the barite veins (Figure 2H,I).

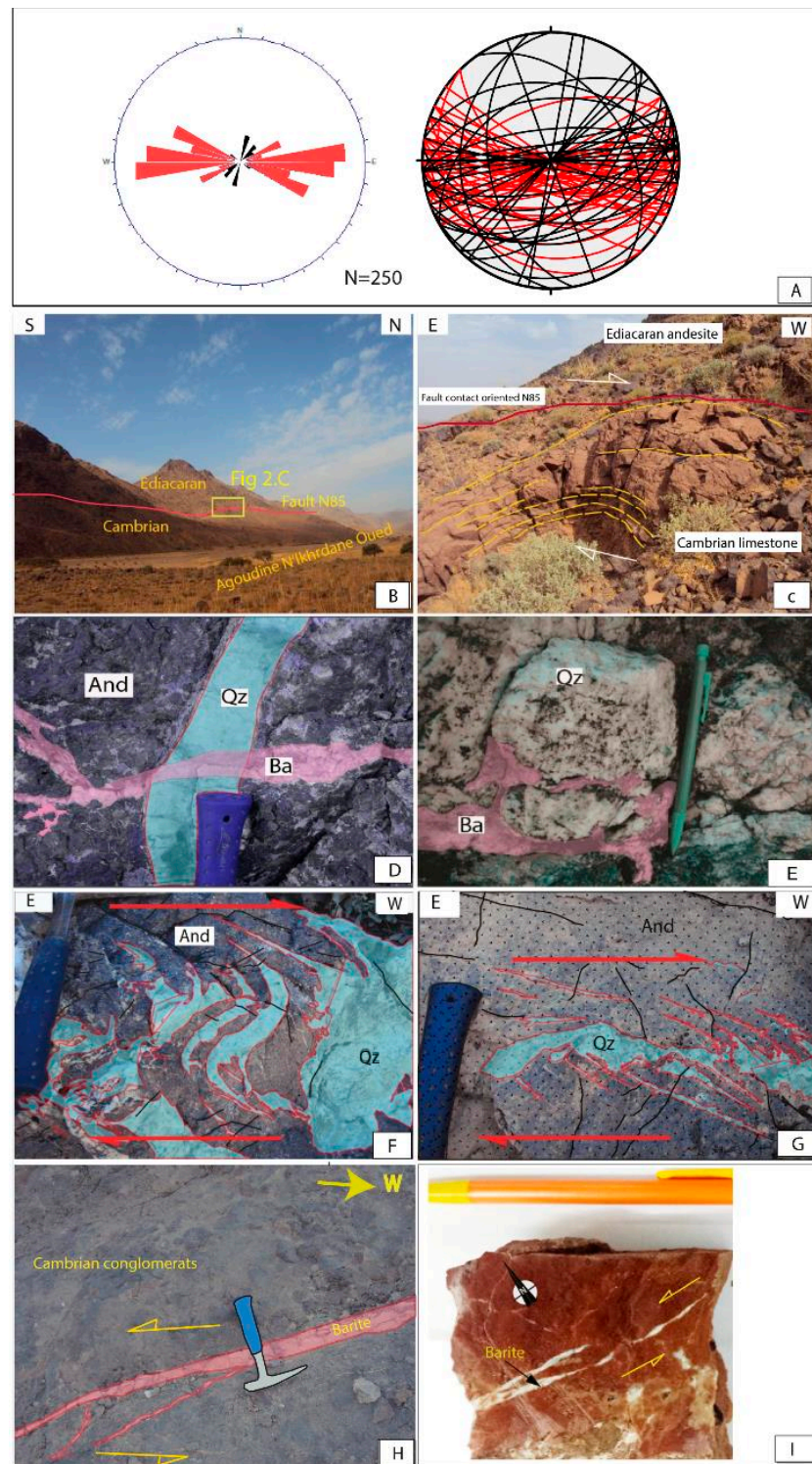


**Figure 2.** (A) Rose diagram and stereographic projection of different tectonic structures mapped at the NE edge of the Saghro inlier ( $n = 250$ ). These tectonic structures include veins (red lines) and faults (black lines). (B,C) Mineralized fault oriented N85, 80 N at the Ediacaran–Cambrian boundary showing folded blocks that indicate dextral movement with a normal component ( $31^{\circ}20'40.96''$  N  $5^{\circ}23'0.38''$  W). (D,E) Crosscutting relationships between barite and quartz veins. (F,G) Quartz veins oriented  $90^{\circ}$  N showing dextral movement, in an Ediacaran andesite host ( $31^{\circ}22.024'$  N  $5^{\circ}26.958'$  W). (H) Barite veins within the Lower Cambrian conglomerate displaying sinistral movement ( $31^{\circ}22'3.09''$  N  $5^{\circ}26'48.98''$  W). (I) Barite veins hosted within lower Cambrian sandstone showing sinistral movement ( $31^{\circ}22'0.11''$  N  $5^{\circ}27'53.27''$  W). Outcrop photos are colored to highlight structural components. And: andesite; Ba: barite; Qz: quartz.

#### 4.1.2. NE–SW-Striking Structures

This fault population is less frequent in the area, and it is mapped within both the Ediacaran and Cambrian rocks. It is represented mainly by fault structures with kilometeric extension; however, no ore veins have been mapped in this population. The faults are oriented from N 30° to N 65°, with a dip between 40° to 90°, generally toward the SE. The chronological relationship suggests that this second system of faults crosscuts the E–W mineralized veins (Figure 3A, B). Tectoglyphs in different fault planes indicate that strike-slip movements are rather sinistral (Figure 3A) or dextral (Figure 3B–D). Furthermore, some other planes have shown a strike-slip sense combined with a normal component (Figure 1C).

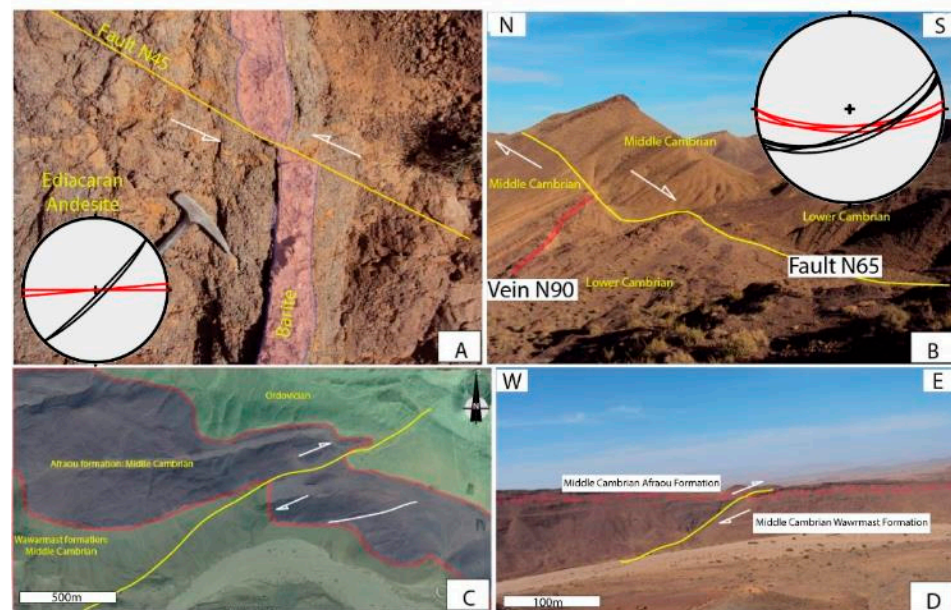


**Figure 3.** (A) Fault oriented N 45° crosscutting a barite vein hosted in Ediacaran andesite. This fault shows sinistral strike-slip movement. For the stereographic projection, the red planes are for veins and the black ones are for faults (31°22′7.77″ N 5°28′1.86″ W). (B) Fault oriented N 65° displaying dextral strike-slip movement. This fault intersects an ore vein that strikes 90° N. This fault shows dextral movement with a normal component. For the stereographic projection, the red planes are for veins and the black ones are for faults (31°22′10.93″ N 5°27′54.17″ W). (C,D) Google Earth and outcrop photos showing a N 50° -oriented dextral strike-slip fault, affecting Middle Cambrian strata (31°21′18.42″ N 5°22′37.80″ W).

#### 4.1.3. NW–SE- to N–S-Striking Structures

This third group of faults, parallel to the hydrographic system, is commonly observed in the NE part of the Saghro inlier.

It corresponds to unmineralized fault systems mapped within Ediacaran and Cambrian formations (Figure 4A–D). These structures generally dip about 70° to 90° to the NW. Tectoglyphs in different fault planes are also observed here, showing strike-slip faulting with either dextral or sinistral motion (Figure 4A–D). A clear crosscutting relationship has been observed between this population of faults and the E–W-striking veins, indicating that these NW–SE to N–S structures are younger (Figure 4D).

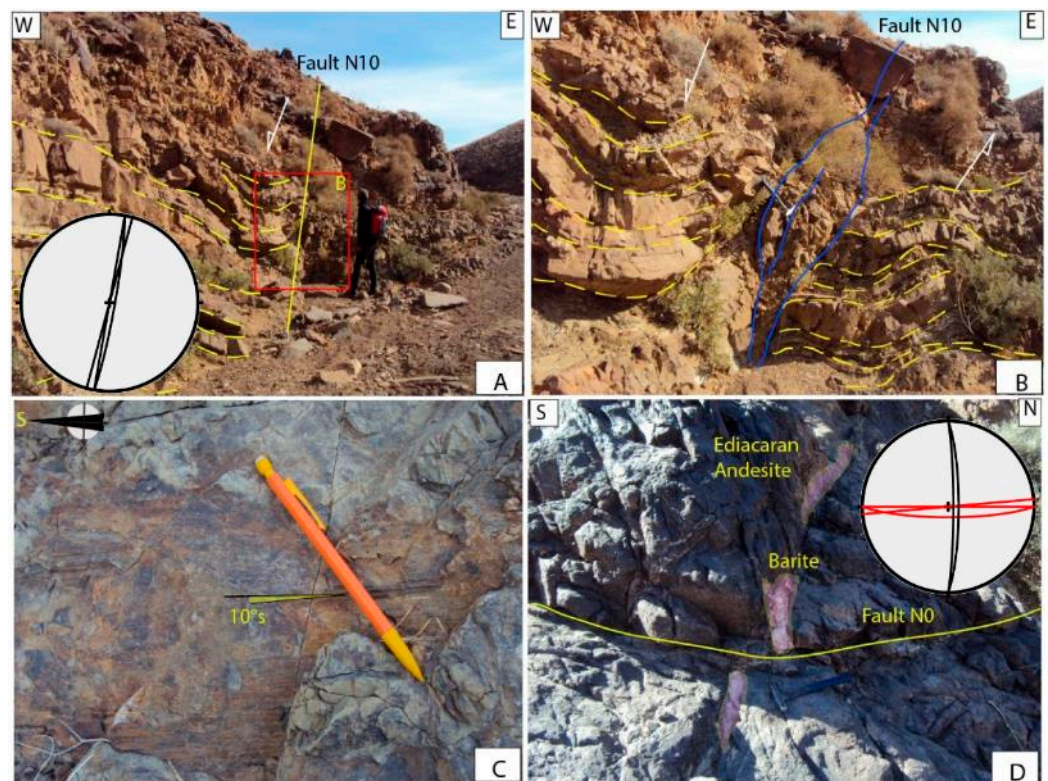


**Figure 4.** (A,B) A N 10° -striking fault system showing sinistral movement ( $31^{\circ}21'48.77''$  N  $5^{\circ}24'58.60''$  W). (C) Slickenside lineations with a pitch of 10° S, developed in a N 5° -striking fault zone. This fault exhibits sinistral strike-slip movement ( $31^{\circ}21'48.77''$  N  $5^{\circ}24'58.60''$  W). (D) Fault oriented N 10° crosscutting a barite vein and showing dextral movement. For the stereographic projection, the red planes are for veins and the black ones are for faults ( $31^{\circ}21'59.15''$  N  $5^{\circ}27'17.89''$  W).

#### 4.2. Microtectonic Analysis

##### 4.2.1. Fractures

- Fractures in the host rocks:

Microtectonic analysis of fracture networks was carried out on various lithofacies including Ediacaran volcano-sedimentary successions and Cambrian sedimentary formations (Figure 5). Additionally, the analysis was extended to ore veins. In the area, the Cambrian formations consist of monoclinical sedimentary series, dipping 20° to 50° towards the north. Based on the frequency, and spatial and temporal relationships, fracture sets are categorized into three groups. The first group comprises E-striking fractures (Figure 5A–H) which occasionally contain barite and/or quartz filling (Figure 5E,F). These microstructures range in length from 1 to several meters and dip steeply to subvertical. They correspond to extension-mode fractures, which are recognized in both Ediacaran and Cambrian rocks. This set of fractures is probably synchronous with the folding of the Paleozoic series during the Variscan orogeny. The second set, represented by NE–SW-striking fractures, is abundant in Ediacaran silica-poor volcanic rocks (Figure 5A–D) and Cambrian sedimentary formations (Figure 5E–H). These fractures exhibit metric length and subvertical dipping, and they correspond to shearing-mode fractures. A clear crosscutting relationship with the first group (E–W-striking fractures) has been documented, confirming that the second group is younger (Figure 5E,G). The third group is the least abundant and comprises NW–SE- to N–S-striking fractures, observed in both Ediacaran volcanic rocks and Cambrian sedimentary formations (Figure 5). Fractures are centimetric to metric in length, steeply dipping to subvertical, and correspond to shearing-mode fractures. A clear crosscutting relationship was also observed between this group and the first one, indicating that the group is younger. However, a relationship between the second and the third groups has not been observed.

Based on the crosscutting relationships, the second and the third sets of fractures are likely associated with tectonic events postdating the Variscan orogeny.

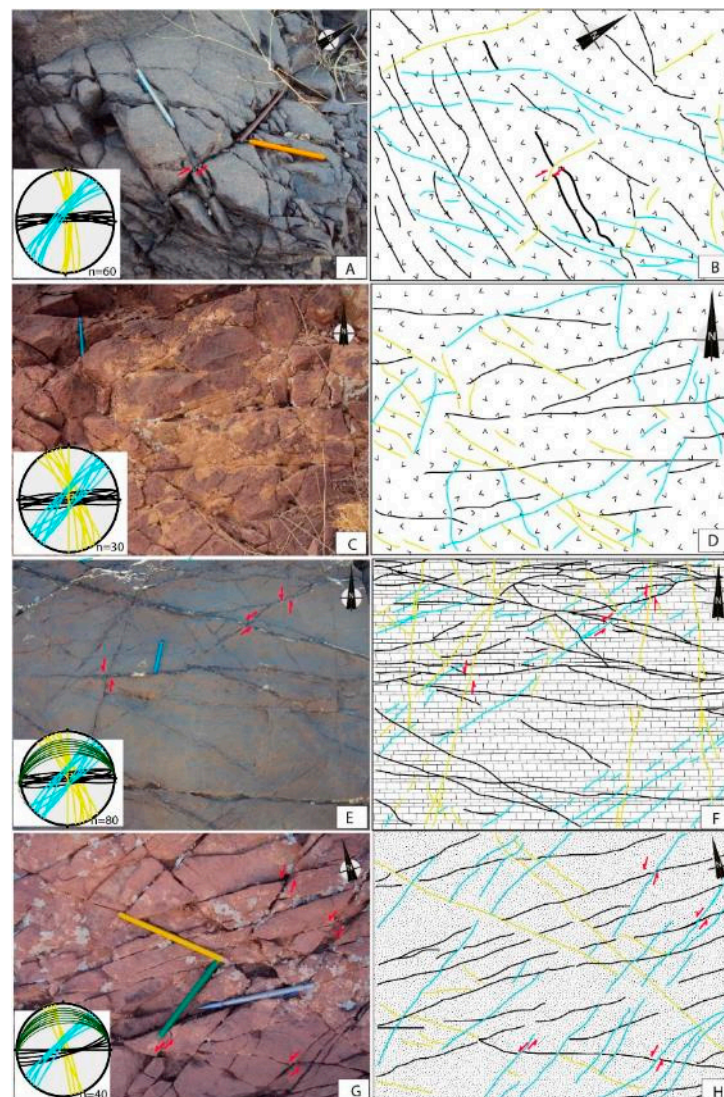


**Figure 5.** (A–D) Field photographs and their sketches showing a fracture network measured within Ediacaran volcanic rocks. (E–H) Photographs and their sketches of a fracture network measured within Cambrian sedimentary facies (carbonate and sandstone, respectively). For the sketches and the stereographic projections, the black lines are for the E–W fractures, the yellow lines are for the NW–SE to N–S fractures, the blue lines mark the NE–SW fractures, and the green lines are for bedding. The coordinates of the different images are (A)  $31^{\circ}21'58.44''$  W  $5^{\circ}27'31.61''$ ; (C)  $31^{\circ}21'55.79''$  N  $5^{\circ}27'28.41''$  W; (E)  $31^{\circ}22'22.59''$  N  $5^{\circ}28'5.04''$  W; (G)  $31^{\circ}22'22.34''$  N  $5^{\circ}28'20.93''$  W.

- Fractures within ore veins:

Fracture analysis within ore veins was conducted in various veins, hosted within both Ediacaran volcanic rocks (Figure 6A–F), Lower Cambrian conglomerates (Figure 6G,H), and limestone (Figure 6I,J).

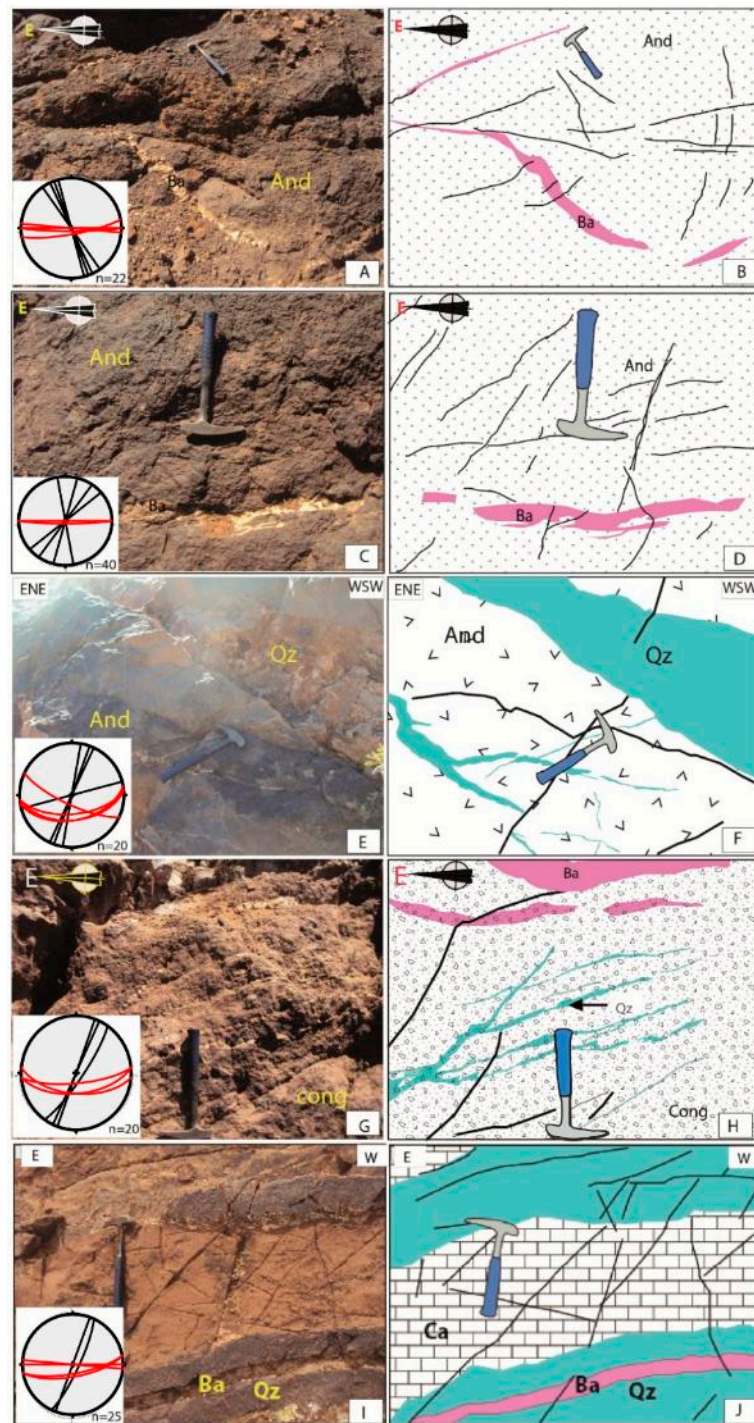
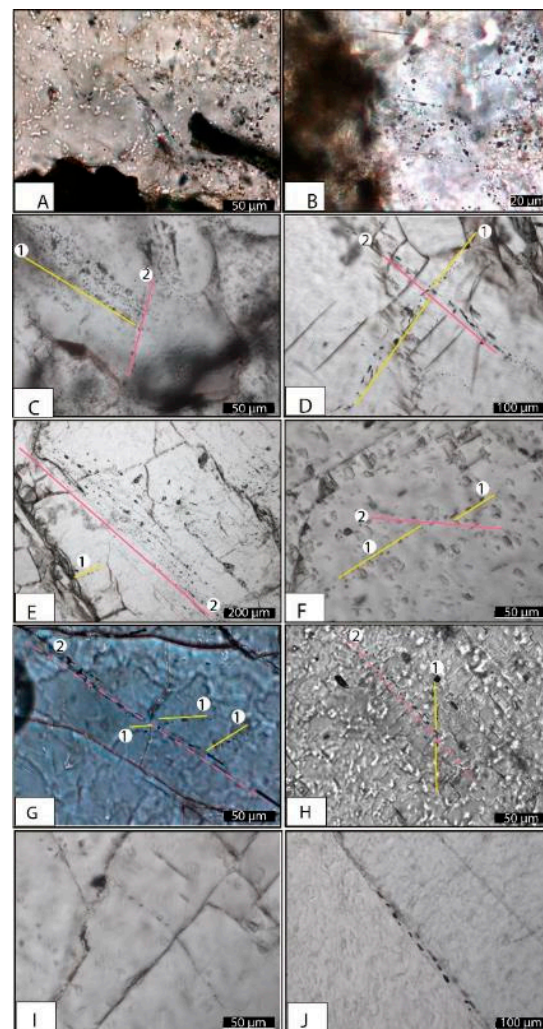


**Figure 6.** (A–D) Field photographs and their sketches depicting a fracture network cutting barite (Ba) veins, hosted by Ediacaran andesite (And). The coordinates of the photographs are (31°21.882' N 5°26.766' W) and (31°21.822' N 5°26.766' W), respectively. (E,F) Field photograph and its sketch showing quartz (Qz) veins hosted in Ediacaran andesite (And) (31°22'1.10'' N 5°26'55.68'' W). (G,H) Field photographs and sketches displaying quartz (Qz) and barite (Ba) veins intersected by fractures, hosted in a Lower Cambrian conglomerate (Cong) (31°21.807' N 5°26.622' W). (I,J) Field photograph and sketch showing barite (Ba) and quartz (Qz) veins hosted in Lower Cambrian limestone (Ca) (31°21.944' N 5°27.864' W). For the stereographic projections, the red planes are for veins, and the black ones are for fractures.

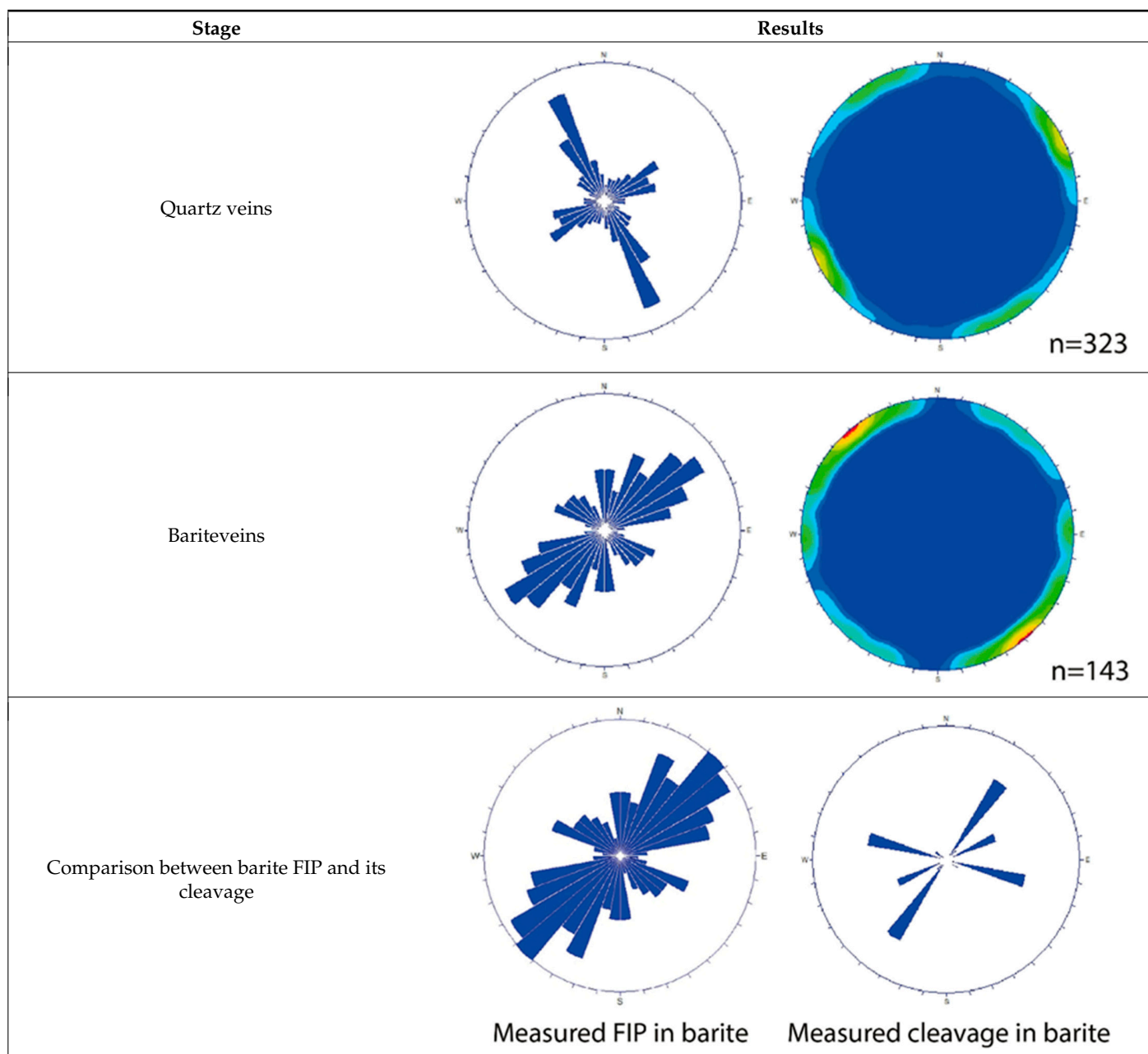
In the area, veins are prominently filled with quartz, barite, calcite, and sulfide or oxides. These veins exhibit an E–W-striking orientation, ranging from  $75^\circ$  N to  $120^\circ$  N. Furthermore, these veins have been intersected by two younger fracture sets. The first comprises NE–SW fractures with orientations ranging from  $30^\circ$  N to  $60^\circ$  N, while the second set is represented by NW–SE to N–S fractures with orientations ranging from  $N 135^\circ$  to  $N 10^\circ$ .

#### 4.2.2. Fluid Inclusion Planes (FIP)

FIP were measured in oriented samples taken from quartz and barite veins (Figure 7, Table 1). The measured FIP results within these veins enable the identification of two distinct orientations, as follows: (i) NE–SW-oriented FIP are more prominent in barite compared to quartz (Figure 7, Table 1). It should be noted that the formation of barite veins occurred after the formation of quartz ones. These FIP indicate NE–SW shortening. (ii) The NW–SE- to N–S-oriented FIP are more abundant in quartz than in barite, resulting from N–S shortening.



**Figure 7.** (A,B) Measured FIP in quartz veins. (C) NE–SW-oriented FIP dissected by NW–SE- to N–S-oriented FIP in quartz veins. (D–H) The relationship between the first and second FIP families in barite. (I) FIP cutting the barite cleavage. (J) FIP parallel to the barite cleavage. The yellow lines and the number 1 in the circle refer to the NE–SW-oriented FIP, and the pink lines and number 2 in the circle refer to the NW–SE- to N–S-oriented FIP.

**Table 1.** Rose diagram and stereographic projections of the obtained results from the measured FIP in barite and quartz veins.

It is important to note that FIP are secondary structures that developed after the crystal growth. Consequently, only the post-quartz and barite tectonism is reflected in the data, which explains the presence of only two FIP orientations: NE–SW and NW–SE to N–S. In addition, based on the relationship between these two FIP groups, the NW–SE- to N–S-oriented FIP is crosscut by the NE–SW ones (Figure 7C–F). Crosscutting relationships have been observed in both quartz and barite (Figure 7C–F), suggesting the superposition of different FIP generations related to post-tectonic events.

## 5. Discussion

### 5.1. Tectonic History of the NE Edge of the Saghro Inlier

As a part of the Anti-Atlas belt, the NE edge of the Saghro inlier is structured by a thick-skinned tectonic style [8,9,19,20]. Previous studies in the area have revealed that the

Ediacaran successions were formed and led by an E–W fault system, mainly with a strike-slip movement. This fault system played a crucial role in controlling the emplacement of Ediacaran magmatic rocks and the associated mineralization during the late Ediacaran time [31–34]. However, according to [5,19,20], most of the Pan-African faults were reactivated during the Variscan to Alpine orogenies. Thus, based on the structural dataset from the NE edge of the Saghro inlier, three fault populations have been distinguished from satellite imagery analysis to fluid inclusion planes. These same fault populations have been identified using Sentinel-2A and Landsat-8 Oli imagery analysis by [35]. However, in this work, most of the mineralized structures in the area were not mapped, and the mineralization–tectonism relationship is missing. These structures are recorded on the Ediacaran rocks and also continue within Cambrian formations, indicating polyphase tectonism in the area during the post-Cambrian tectonic events (Figure 8). The main tectonic structures are represented by inherited major E–W-striking tectonic structures, including faults, fractures, and veins. The latter are filled with quartz, barite, calcite, and sulfide or oxide mineralization [36]. These structures show strike-slip movements that reveal the existence of at least two tectonic events: first, they acted as dextral syn-kinematic with quartz veins, followed by sinistral movement syn-kinematic with barite veins. On a broad scale, E–W structures have been reported within the Saghro Group metasedimentary units in the neighboring area to the east of the studied area, especially in the Imiter, Boumalne, and Kalaat M’Gouna sub-inliers [15,18,32,37,38]. These faults were assumed to represent Ediacaran tectonic structures that were associated with an important stock of mineralization [34,39]. It should be noted that the dextral E–W-striking structures also continue into Paleozoic formations, which indicates that they were reactivated during the Variscan or Alpine orogenies [5,19,20]. In addition, the presence of the Ag–Hg–Cu Tassafté deposits in Ediacaran–Cambrian formations [36] and a young age at  $254.7 \pm 3.2$  Ma [40] attributed to the Ag–Hg Imiter deposits makes an Ediacaran age for these structures very unlikely. Similarly, a dextral transpression regime has been reported by [24] on the NE edge of the Saghro inlier (Figure 8A), within the Ordovician–Carboniferous formations in the Tilouine and Ouaklim units (Figure 8A). The thick-skinned tectonic style (D2 phase) led to the development of large-scale antiforms and synforms in the Ouaklim and Tilouine units [24]. According to the same author, this deformation episode is attributed to the Neovariscan tectonics during 300–290 Ma. Further to the west, in the Bas Draa inlier, the same tectonic event has been reported within the Azougar n’Tilili ore deposit, where the Au–Ag mineralization is hosted within Cambrian sediments and assumed to be related to Variscan dextral transpression [41,42]. This phase is equivalent to the oblique convergence observed in the whole Moroccan Variscides [25]. Thus, the dextral E–W-striking faults on the NE edge of the Saghro inlier could be related to the Neovariscan tectonism (Figure 8).

The sinistral regime of the major E–W-striking faults depicted in the barite veins hosted in the Precambrian–Cambrian formations has been recognized in the Late Ediacaran succession in the Skoura-Sidi Flah dyke swarm zone [18]. The barite mineralization within the Anti-Atlas belt is widely attributed to the Late Paleozoic–Lower Triassic tectonic episode, which coincided with the opening of the Central Atlantic Ocean, for instance, at the Ras El Hamda mine in the Ougnat inlier [43], and the Oumjrane-Bounhass mine within Ordovician formations in eastern Anti-Atlas [43]. In addition, the same age has been attributed to the Tadaout-Tizi n’Rsas Cu–Pb–Zn–Ba deposits, located in the easternmost Anti-Atlas [44]. On the eastern margin of the Saghro inlier, the same left-lateral transtensional regime has also been described along the E–W-striking Tizi n’Boujou and Bou Larhzazil-Tinifift Faults [9] (Figure 8B). The kinematic of these faults was related to the tectonic phase D1 reported from [9] which took place during the Triassic rifting of Pangea, and to an Early–Middle Jurassic transtensional tectonics dated on the basis of fission tracks at  $216 \pm 11$  Ma. This phase was also associated with the emplacement of NE–SW tholeiitic dykes of the Early Jurassic age (e.g., Foum Zguid; [45,46]). Further north of the Saghro inlier, in the Skoura inlier, central High Atlas, a left-lateral movement has been documented in the area during the Triassic time, and these faults are assumed to be controlled by the evolution of Triassic

basins in the central High Atlas [47]. Consequently, the left-lateral tectonic phase observed within the E–W-striking faults is likely related to the Mesozoic tectonism in association with the Triassic rifting of Pangea (Figure 9). Later, the E–W tectonic structures were segmented by two tectonic phases, which are oriented NE–SW and NW–SE to N–S (Figure 8C,D). They are represented by fault systems, measured in Ediacaran volcanic rocks and Cambrian formations as well. They are also recognized by FIP analyzed in quartz and barite veins. Based on the measured FIP, the NW–SE to N–S lineaments correspond to the late tectonic phases recorded on the NE edge of the Saghro inlier. Our finding is in line with two thick-skinned phases obtained on the basis of fission-track (FT) analysis on apatite by [9] (Figure 8C,D). The first tectonic stage is coeval with the development of the NE–SW faulting system and probably corresponds to inherited structures, which were reactivated during D2. This phase is assumed to be linked to the Neogene NW–SE compression that resulted in NE–SW tensional joints and dextral reactivation of previous faults [9]. On the other hand, the NW–SE to N–S fault structures are consistent with the latest tectonic phases, D3 and D4, reported by [9] (Figure 8C,D and Figure 9); these took place during the Late Neogene to Quaternary, and correspond to N–S compression.

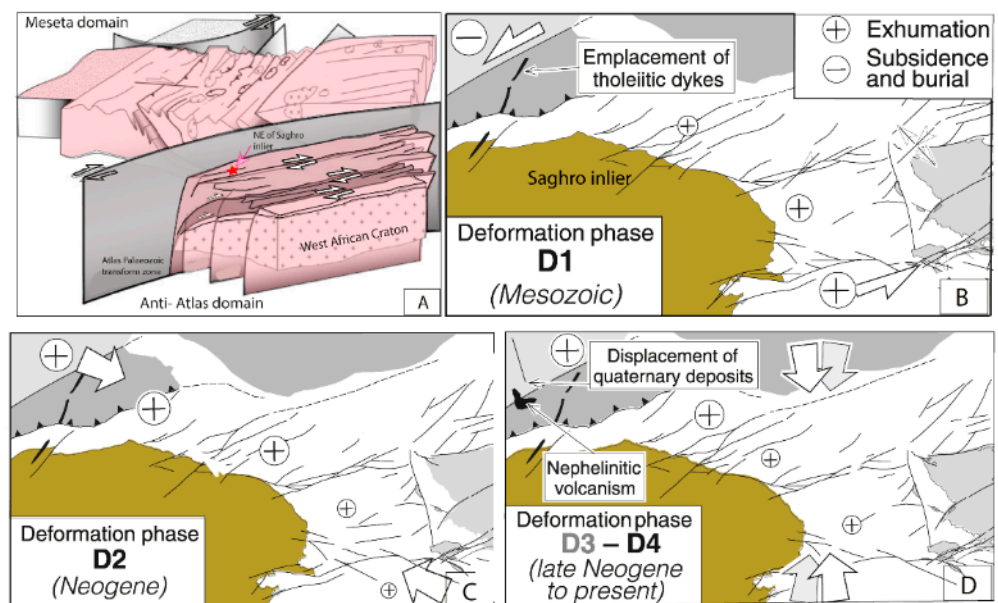


**Figure 8.** Different tectonic phases recorded on the NE edge of the Saghro inlier. (A) Geodynamic model during the Variscan modified after [25]. (B–D) Post-Variscan tectonic evolution of the eastern Anti-Atlas. Plus and minus indicate blocks characterized by exhumation and burial, respectively, with size proportional to the relative rate. White and grey arrows represent the kinematic movement (after [9]).

The above-discussed results from different tectonic structures recorded in the area resulted from multiple tectonic phases. The results are crucial for mining exploration and exploitation since the data show that the ore deposits in the area are Eao-variscan to Triassic age, which could be a metallotect in ore exploration in the area.

### 5.2. Phanerozoic Tectono-Magmatic–Hydrothermal Evolution of the Anti-Atlas Mountains

The Anti-Atlas Mountains are believed to have evolved during a long geological history, resulting from different orogenies, including the Eburnean and Panafrican during Precambrian time, and then the Variscan and Atlasic during the Phanerozoic (Figure 9). Such a tectono-thermal telescoped evolution caused polycyclic hydrothermalism that would explain the complicity and diversity of ore deposits in the Anti-Atlas belt [43,48,49]. During the Phanerozoic time, several tectono-magmatic and hydrothermal events have been recorded on the Anti-Atlas belt. The Cambrian is known from an important alkaline

to tholeiitic magmatism identified in the Anti-Atlas, especially in the Kerdous, Bou Azzer, and Ougnat inliers, and related to the opening of the Iapetus ocean [2,50–52].

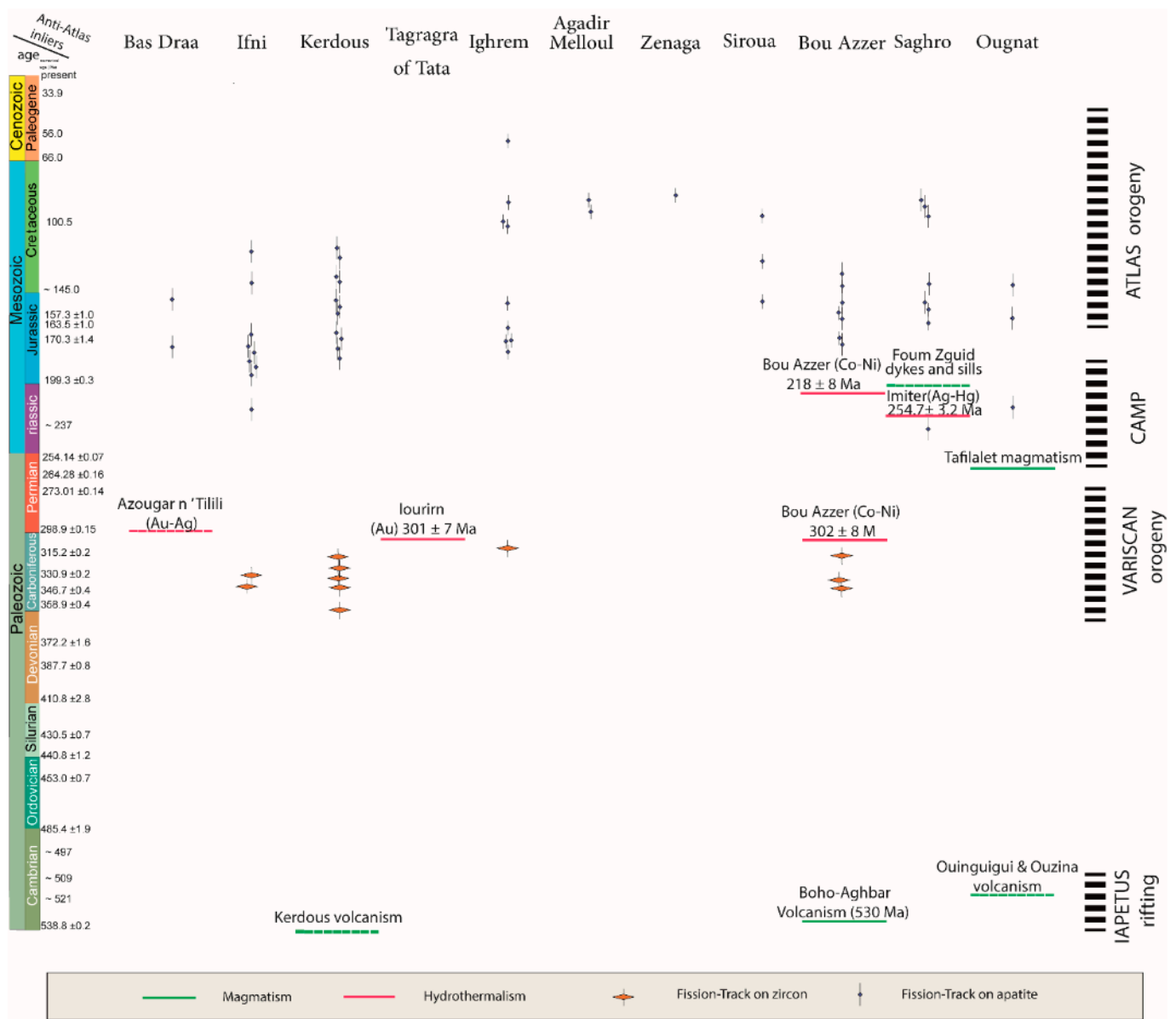


**Figure 9.** Tectono-magmatic–hydrothermal chart of the Anti-Atlas Mountains. The data are collected from [6,9–12,34,41,42,45,51–60]. Discontinuous lines are for interpretative data while continuous lines are for data based on age dating. For the Geological time, we used the ICS International Chronostratigraphic Chart 2022. CAMP: Central Atlantic Magmatic Province.

Later, during the Variscan orogeny (Lower Carboniferous to Lower Permian) the Paleozoic Anti-Atlas basins were deformed and folded, while according to results depicted from fission tracks on zircons, large blocks of the Precambrian basement were uplifted as inliers [5,6,10,11]. During the Variscan orogeny, significant hydrothermal activity has been reported in the Anti-Atlas, related to several ore deposits, e.g., The Au Aouriri deposit (Tagragra of Akka inlier), and the Co–Ni–Ag–Au Bou Azzer deposit (Bou Azzer inlier) [54,56]. In the Middle to Upper Permian, an important magmatism is reported in the Tafilalet area [59] representing an early stage of Triassic rifting that is heralded by the Central Atlantic Magmatic Province (CAMP) during Triassic time. In the Anti-Atlas, the CAMP is represented by sills and dykes mainly mapped in the South of the Saghro inlier [45,46]. This magmatism conduct to a noteworthy hydrothermalism that led to several ore deposits

stocks, e.g., the Ag–Hg Imiter deposits (Saghro inlier) [40], the Co–Ni–Ag–Au Bou Azzer deposits (Bou Azzer inlier) [34], and the Ba–Fa Ras Elhamda deposits (Ougnat inlier) [43]. Later, during the Alpine orogeny in which the Atlasic domain was inverted and uplifted, the Anti-Atlas was coevally exhumed [6,9–11]. In the Neogene time, an important alkaline magmatism is reported which crops out in the Saghro and Siroua inliers [61,62]. The uranium deposit in the Zgounder area is related to this magmatism [63].

## 6. Conclusions

A multiscale structural analysis, ranging from field mapping analysis to fluid inclusion planes, was conducted on Ediacaran–Cambrian rocks, on the NE edge of the Saghro inlier. The obtained results from various scales exhibit a remarkable coherence and emphasize the presence of multiple tectonic phases recorded in the area. Consequently, three populations have been reported here as a result of four tectonic events.

- The first set comprises E–W-striking structures, which are the main features observed in the area. These structures represent the host ore bodies (sulfides, oxide, barite, and quartz) in the area that intersects the Ediacaran–Cambrian rocks. These structures exhibit evidence of polyphase tectonism, initially manifesting as dextral strike-slip syn-kinematic movements with associated quartz veins, resulting from NW–SE shortening. This tectonic phase is believed to be equivalent to the Neovariscan tectonics (300–290 Ma). The same E–W-striking structures were subsequently reactivated during the Mesozoic tectonic phases, as sinistral movements attributed to the NE–SW shortening, and contemporary with the formation of barite mineralization.
- The second group of NE–SW faults crosscuts the E–W structures. These faults exhibit both dextral and sinistral strike-slip motion, likely related to the Neogene NW–SE shortening.
- The last tectonic event in the area is characterized by NW–SE to N–S-striking faults, that cut the E–W mineralized structures. They correspond to strike-slip faults that are linked to NW–SE to N–S shortening during the Late Neogene to Quaternary tectonism.

**Author Contributions:** Conceptualization, investigation, methodology, writing—original draft preparation, software, and resources, Z.Y.; methodology, visualization, investigation, writing—original draft preparation, and software, H.S. and C.C.; conceptualization, investigation, and writing—original draft preparation, B.K.; conceptualization and investigation, A.K.; investigation and supervision, A.M., H.E.O. and L.B. All authors have read and agreed to the published version of the manuscript.

**Funding:** This research was partly supported by Erasmus Mobile 2+ within the framework of Moulay Ismail–Porto universities cooperation. In this framework, the first author (Z.Y) benefited from a mobility grant from Porto University thanks to which fluid inclusion planes were measured. C.C is a contracted researcher under the UIDP/04683/2020 project (Fundação para Ciência e a Tecnologia, Portugal). This work was supported by national funding awarded by FCT—Foundation for Science and Technology, I.P., projects UIDB/04683/2020 and UIDP/04683/2020.

**Data Availability Statement:** Not applicable.

**Acknowledgments:** Z.Y. expresses his heartfelt gratitude to the Ancemar mining company for their logistics support in the field studies. We extend warm gratitude to Raymundo Casas–García and Boris Chako Tchamabe for their help in improving the English style. The authors also wish to express sincere appreciation to the three anonymous reviewers for their insightful and constructive review comments.

**Conflicts of Interest:** The authors declare no conflict of interest.

## References

1. Thomas, R.J.; Fekkak, A.; Ennih, N.; Errami, E.; Loughlin, S.C.; Gresse, P.G.; Chevallier, L.P.; Liégeois, J.P. A New Lithostratigraphic Framework for the Anti-Atlas Orogen, Morocco. *J. Afr. Earth Sci.* **2004**, *39*, 217–226. [[CrossRef](#)]
2. Gasquet, D.; Levresse, G.; Cheilletz, A.; Azizi-Samir, M.R.; Mouttaqi, A. Contribution to a Geodynamic Reconstruction of the Anti-Atlas (Morocco) during Pan-African Times with the Emphasis on Inversion Tectonics and Metallogenic Activity at the Precambrian-Cambrian Transition. *Precambrian Res.* **2005**, *140*, 157–182. [[CrossRef](#)]

3. Michard, A.; de Lamotte, D.F.; Liégeois, J.P.; Saddiqi, O.; Chalouan, A. Conclusion: Continental Evolution in Western Maghreb. *Lect. Notes Earth Sci.* **2008**, *116*, 395–404. [[CrossRef](#)]
4. Soulaïmani, A.; Burkhard, M. The Anti-Atlas Chain (Morocco): The Southern Margin of the Variscan Belt along the Edge of the West African Craton. *Geol. Soc. Lond. Spec. Publ.* **2008**, *297*, 433–452. [[CrossRef](#)]
5. Soulaïmani, A.; Michard, A.; Ouanaimi, H.; Baidder, L.; Raddi, Y.; Saddiqi, O.; Rjimati, E.C. Late Ediacaran-Cambrian Structures and Their Reactivation during the Variscan and Alpine Cycles in the Anti-Atlas (Morocco). *J. Afr. Earth Sci.* **2014**, *98*, 94–112. [[CrossRef](#)]
6. Gouiza, M.; Charton, R.; Bertotti, G.; Andriessen, P.; Storms, J.E.A. Post-Variscan Evolution of the Anti-Atlas Belt of Morocco Constrained from Low-Temperature Geochronology. *Int. J. Earth Sci.* **2017**, *106*, 593–616. [[CrossRef](#)]
7. Choubert, G. Histoire Géologique Du Domaine de l'Anti-Atlas. *Notes Mémoires Serv. Géologique* **1952**, *100*, 196.
8. Michard, A. Eléments de Géologie Marocaine. *Notes Mem. Serv. Geol.* **1976**, *552*, 408.
9. Malusà, M.G.; Polino, R.; Feroni, A.C.; Ellero, A.; Ottria, G.; Baidder, L.; Musumeci, G. Post-Variscan Tectonics in Eastern Anti-Atlas (Morocco). *Terra Nov.* **2007**, *19*, 481–489. [[CrossRef](#)]
10. Oukassou, M.; Saddiqi, O.; Barbarand, J.; Sebti, S.; Baidder, L.; Michard, A. Post-Variscan Exhumation of the Central Anti-Atlas (Morocco) Constrained by Zircon and Apatite Fission-Track Thermochronology. *Terra Nov.* **2013**, *25*, 151–159. [[CrossRef](#)]
11. Charton, R.; Bertotti, G.; Arantegui, A.; Bulot, L. The Sidi Ifni Transect across the Rifted Margin of Morocco (Central Atlantic): Vertical Movements Constrained by Low-Temperature Thermochronology. *J. Afr. Earth Sci.* **2018**, *141*, 22–32. [[CrossRef](#)]
12. Sehr, M.; Glasmacher, U.A.; Stockli, D.F.; Jabour, H.; Kluth, O. The Southern Moroccan Passive Continental Margin: An Example of Differentiated Long-Term Landscape Evolution in Gondwana. *Gondwana Res.* **2018**, *53*, 129–144. [[CrossRef](#)]
13. Ruiz, G.M.H.; Sebti, S.; Negro, F.; Saddiqi, O.; Frizon De Lamotte, D.; Stockli, D.; Foeken, J.; Stuart, F.; Barbarand, J.; Schaer, J.P. From Central Atlantic Continental Rift to Neogene Uplift-Western Anti-Atlas (Morocco). *Terra Nov.* **2011**, *23*, 35–41. [[CrossRef](#)]
14. Hindermeyer, J. Carte Géologique Du Jbel Saghro-Dades Au 1/200.000. *Notes Mém. Serv. Geol. Maroc* **1977**, 161.
15. Fekkak, A.; Pouclet, A.; Ouguir, H.; Ouazzani, H.; Badra, L.; Gasquet, D. Géochimie et Signification Géotectonique Des Volcanites Du Cryogénien Inférieur Du Saghro (Anti-Atlas Oriental, Maroc)/Geochemistry and Geotectonic Significance of Early Cryogenian Volcanics of Saghro (Eastern Anti-Atlas, Morocco). *Geodin. Acta* **2001**, *14*, 373–385. [[CrossRef](#)]
16. Ouguir, H. Contexte Géologique Du Gisement Argentifère d'Imiter (Anti-Atlas Oriental, Maroc). Contrôle Volcanique et Structural de la Mise en Place des Concentrations Métalliques à Ag-Hg. Unpublished Thesis, University of Meknes, Meknes City, Morocco, 1997.
17. Errami, E.; Linnemann, U.; Hofmann, M.; Gärtner, A.; Gärtner, J.; Mende, K.; El Kabouri, J.; Gasquet, D.; Ennih, N. From Pan-African Transpression to Cadomian Transtension at the West African Margin: New U-Pb Zircon Ages from the Eastern Saghro Inlier (Anti-Atlas, Morocco). *Geol. Soc. London* **2020**, *503*, 209–233. [[CrossRef](#)]
18. Walsh, G.J.; Benziane, F.; Aleinikoff, J.N.; Harrison, R.W.; Yazidi, A.; Burton, W.C.; Quick, J.E.; Saadane, A. Neoproterozoic Tectonic Evolution of the Jebel Saghro and Bou Azzer-El Graara Inliers, Eastern and Central Anti-Atlas, Morocco. *Precambrian Res.* **2012**, *216–219*, 23–62. [[CrossRef](#)]
19. Schiavo, A.; Taj Eddine, K.; Algouti, A.H.; Benvenuti, M.; Eddebbi, A.; El Boukhari, A.; Laftouhi, N.; Massironi, M.; Dal Piaz, G.V.; Moratti, G.; et al. *Carte Géologique Du Maroc Au 1/50 000 FEUILLE IMTIR*; n 518 bis; Notes et Mémoires du Service Géologique; Maroc, 2007; ISBN 9954884637.
20. Schiavo, A.; Taj Eddine, K.; Algouti, A.H.; Benvenuti, M.; Eddebbi, A.; El Boukhari, A.; Laftouhi, N.; Massironi, M.; Dal Piaz, G.V.; Moratti, G.; et al. *Carte Géologique Du Maroc Au 1:50 000 FEUILLE TAGHAZOUT*; n 519 bis; Notes et Mémoires du Service Géologique; 2007; ISBN 9954884629.
21. Massironi, M.; Moratti, G.; Algouti, A.H.; Benvenuti, M.; Dal Piaz, G.V.; Eddebbi, A.; El Boukhari, A.; Laftouhi, N.; Ouanaimi, H.; Schiavo, A. *Carte Géologique Du Maroc Au 1/50 000, Feuille Boumalne*. *Notes Mémoires du Serv. Géologique du Maroc* **2007**, *521*, 80.
22. Yajjoui, Z.; Karaoui, B.; Chew, D.; Breikreuz, C.; Mahmoudi, A. U–Pb Zircon Geochronology of the Ediacaran Volcano-Sedimentary Succession of the NE Saghro Inlier (Anti-Atlas, Morocco): Chronostratigraphic Correlation on the Northwestern Margin of Gondwana. *Gondwana Res.* **2020**, *87*, 263–277. [[CrossRef](#)]
23. Yajjoui, Z. Ediacaran–Cambrian Evolution of the Northeastern Edge of Saghro Inlier (Eastern Anti-Atlas, Morocco): Insights from Physical Structural Analysis and Metallogenic Implication. Ph.D. Thesis, Geology Department, Moulay Ismail University, Meknes, Morocco, 2019.
24. Cerrina Feroni, A.; Ellero, A.; Malusà, M.G.; Musumeci, G.; Ottria, G.; Polino, R.; Leoni, L. Transpressional Tectonics and Nappe Stacking along the Southern Variscan Front of Morocco. *Int. J. Earth Sci.* **2010**, *99*, 1111–1122. [[CrossRef](#)]
25. Hoepffner, C.; Houari, M.R.; Bouabdelli, M. Tectonics of the North African Variscides (Morocco, Western Algeria): An Outline. *Comptes Rendus Geosci.* **2006**, *338*, 25–40. [[CrossRef](#)]
26. Gasquet, D.; Ennih, N.; Liégeois, J.P.; Soulaïmani, A.; Michard, A. The Pan-African Belt. In *Lecture Notes in Earth Sciences*; Springer: Berlin/Heidelberg, Germany, 2008; Volume 116, pp. 33–64, Chapter 2, ISBN 9783540770756.
27. Lespinasse, M.; Pêcher, A. Microfracturing and Regional Stress Field: A Study of the Preferred Orientations of Fluid-Inclusion Planes in a Granite from the Massif Central, France. *J. Struct. Geol.* **1986**, *8*, 169–180. [[CrossRef](#)]
28. Sheperd, T.J. Geological Link Between Fluid Inclusion, Dilatant Microcracks, and Palaeostress Field. *J. Geophys. Res.* **1990**, *95*, 11115–11120. [[CrossRef](#)]

29. Sant’Ovaia, H.; Nogueira, P.; Lopes, J.C.; Gomes, C.; Ribeiro, M.A.; Martins, H.C.B.; Dória, A.; Cruz, C.; Lopes, L.; Sardinha, R.; et al. Building up of a Nested Granite Intrusion: Magnetic Fabric, Gravity Modelling and Fluid Inclusion Planes Studies in Santa Eulália Plutonic Complex (Ossa Morena Zone, Portugal). *Geol. Mag.* **2015**, *152*, 648–667. [[CrossRef](#)]
30. Lespinasse, M.; Cathelineau, M. Paleostress Magnitudes Determination by Using Fault Slip and Fluid Inclusions Planes Data. *J. Geophys. Res.* **1995**, *100*, 3895–3904. [[CrossRef](#)]
31. Errami, E.; Bonin, B.; Laduron, D.; Lasri, L. Petrology and Geodynamic Significance of the Post-Collisional Pan-African Magmatism in the Eastern Saghro Area (Anti-Atlas, Morocco). *J. Afr. Earth Sci.* **2009**, *55*, 105–124. [[CrossRef](#)]
32. Ouguir, H.; Macaudiere, J.; Dagallier, G. Le Protérozoïque Supérieur d’Imiter, Saghro Oriental, Maroc: Un Contexte Géodynamique d’arrière-Arc. *J. Afr. Earth Sci.* **1996**, *22*, 173–189. [[CrossRef](#)]
33. Tuduri, J. Processus de Formation et Relations Spatio-Temporelles Des Minéralisations à or et Argent En Contexte Volcanique Précambrien (Jbel Saghro, Anti-Atlas, Maroc). Implications Sur Les Relations Déformation-Magmatisme- Volcanisme-Hydrothermalisme, 2005. Available online: <https://www.semanticscholar.org/paper/Processus-de-formation-et-relations-des-C3%A0-or-et-en-Tuduri/8c68aa171f62a5402f2d2384448983312e5ea381> (accessed on 28 May 2023).
34. Levresse, G. Contribution à l’établissement d’un Modèle Génétique Des Gisements d’Imiter (Ag-Hg), Bou Madine (Pb-Zn-Cu-Ag-Au) et Bou Azzer (Co-Ni-As-Au-Ag) Dans l’Anti-Atlas Marocain. Ph.D. Thesis, Institut National Polytechnique de Lorraine (INPL), Nancy, France, 2001.
35. Hejja, Y.; Baidder, L.; Ibouh, H.; Bba, A.N.; Soulaïmani, A.; Gaouzi, A.; Maacha, L. Fractures Distribution and Basement-Cover Interaction in a Polytecnic Domain: A Case Study from the Saghro Massif (Eastern Anti-Atlas, Morocco). *J. Afr. Earth Sci.* **2020**, *162*, 103694. [[CrossRef](#)]
36. Yajoui, Z.; Badra, L.; Mahmoudi, A.; Lima, A.; Karaoui, B. New Occurrence of Ag-Hg-Cu Mineralization in the Tassafta Area, NE Edge of the Saghro Inlier, Ediacaran- Cambrian Transition (Eastern Anti-Atlas, Morocco). In Proceedings of the 15th Biennial SGA Meeting, Glasgow, UK, 27–30 August 2019; pp. 1–4.
37. Tuduri, J.; Chauvet, A.; Ennaciri, A.; Barbanson, L. Modèle de Formation Du Gisement d’argent d’Imiter (Anti-Atlas Oriental, Maroc). Nouveaux Apports de l’analyse Structurale et Minéralogique. *Comptes Rendus-Geosci.* **2006**, *338*, 253–261. [[CrossRef](#)]
38. Hejja, Y.; Bourdier, J.L.; Gaouzi, A.; Baidder, L.; Tuduri, J.; Ennaciri, A.; Zakir, A.; Maachaa, L.; Zouhair, M. Lithostratigraphy and Structural Framework of the Ediacaran Volcano-Plutonic Complex of the Imiter Ag-Hg Mining District (Jbel Saghro, Anti-Atlas, Morocco). *J. African Earth Sci.* **2022**, *196*, 104687. [[CrossRef](#)]
39. Ouguir, H.; Macaudiere, J.; Dagallier, G.; Qadrouci, A.; Leistel, J.M. Cadre Structural Du Gite Ag-Hg d’Imiter (Anti Atlas, Maroc); Implication Metallogénique. *Bull. Soc. Geol. Fr.* **1994**, *165*, 233–248.
40. Borisenko, A.S.; Lebedev, V.I.; Borovikov, A.A.; Pavlova, G.G.; Kalinin, Y.A.; Nevol’ko, P.A.; Maacha, L.; Kostin, A.V. Forming Conditions and Age of Native Silver Deposits in Anti-Atlas (Morocco). *Dokl. Earth Sci.* **2014**, *456*, 663–666. [[CrossRef](#)]
41. Karaoui, B. Geodynamic Evolution of the Bas Draâ Inlier (Western Anti-Atlas, Morocco): Insights from Physical Volcanology, Geochemistry and Geochronology of the Ediacaran Volcanosedimentary Successions and Structural Analysis of Variscan Deformation. Ph.D. Thesis, Faculty of Sciences, Moulay Ismail University, Meknès, Morocco, 2014.
42. Hasnaoui, A.E.L.; Soulaïmani, A.; Maacha, L.; Michard, A.; Saddiqi, O.; Maidani, A.E.L. Azougar n’ Tilili, Nouveau Gîte Polymétallique Aurifère Dans Le Cambrien Du Azougar n’ Tilili, a New Gold-Rich Polymetallic Prospect in the Bas-Draa Cambrian Formations (Western Ant-Atlas). *Nouv. Guides Géologiques Min. Maroc* **2011**, *9*, 564.
43. Mouttaqi, A.; Rjimati, E.C.; Maacha, L.; Michard, A.; Soulaïmani, A.; Ibouh, H. *Les Principales Mines du Maroc/Main Mines of Morocco*; Éditions du Service Géologique du Maroc: Rabat, Maroc, 2011; Volume 9.
44. Ait Daoud, M.; Essalhi, A.; Essalhi, M.; Toummite, A. The Role of Variscan Shortening in the Control of Mineralization Deposition in Tadaout-Tizi N’rsas Mining District (Eastern Anti-Atlas, Morocco). *Bull. Miner. Res. Explor.* **2020**, *161*, 13–32. [[CrossRef](#)]
45. Bouiflane, M.; Manar, A.; Medina, F.; Youbi, N.; Rimi, A. Mapping and Characterization from Aeromagnetic Data of the Fom Zguid Dolerite Dyke (Anti-Atlas, Morocco) a Member of the Central Atlantic Magmatic Province (CAMP). *Tectonophysics* **2017**, *708*, 15–27. [[CrossRef](#)]
46. Marzoli, A.; Callegaro, S.; Dal Corso, J.; Davies, J.H.F.L.; Chiaradia, M.; Youbi, N.; Bertrand, H.; Reisberg, L.; Merle, R.; Jourdan, F. *The Central Atlantic Magmatic Province (CAMP): A Review*; Springer: Cham, Switzerland, 2018; ISBN 978-3-319-02903-0.
47. Laville, E.; Petit, J.P. Role of Synsedimentary Strike-Slip Faults in the Formation of Moroccan Triassic Basins. *Geology* **1984**, *12*, 424–427. [[CrossRef](#)]
48. Barodi, E.B.; Watanabe, Y.; Mouttaqi, A.; Annich, M. Méthodes Et Techniques D’Exploration Minière et Principaux Gisements Au Maroc. Projet JICA/BRPM, 2002.
49. Marcoux, É.; Jébrak, M. Plombotectonique Des Gisements Du Maroc. *Bull. Société Géologique Fr.* **2021**, *192*, 32. [[CrossRef](#)]
50. Pouclet, A.; El Hadi, H.; Alvaro, J.; Bardintzeff, J.M.; Benharref, M.; Fekkak, A. Review of the Cambrian Volcanic Activity in Morocco: Geochemical Fingerprints and Geotectonic Implications.... Review of the Cambrian Volcanic Activity in Morocco: Geochemical Fingerprints and Geotectonic Implications for the Rifting of West. *Int. J. Earth Sci.* **2018**, *107*, 2101–2123. [[CrossRef](#)]
51. Brauner, J.; Arndt, M.; Yajoui, Z.; Karaoui, B.; Breitkreuz, C.; Mahmoudi, A. Cambrian Shallow-Marine to Emergent Alkaline Volcanism near Ouinguigui (Ougnat Inlier, Eastern Anti-Atlas, Morocco): Volcanic Facies, Geochemistry and Geodynamic Setting. *J. Afr. Earth Sci.* **2020**, *161*, 103581. [[CrossRef](#)]

52. Álvaro, J.J.; Ezzouhairi, H.; Vennin, E.; Ribeiro, M.L.; Clausen, S.; Charif, A.; Ayad, N.A.; Moreira, M.E. The Early-Cambrian Boho Volcano of the El Graara Massif, Morocco: Petrology, Geodynamic Setting and Coeval Sedimentation. *J. Afr. Earth Sci.* **2006**, *44*, 396–410. [[CrossRef](#)]
53. Soulaïmani, A.; Essaïfi, A.; Youbi, N.; Hafid, A. Les Marqueurs Structuraux et Magmatiques de l'extension Crustale Au Protérozoïque Terminal-Cambrien Basal Autour Du Massif de Kerdous (Anti-Atlas Occidental, Maroc). *Comptes Rendus Geosci.* **2004**, *336*, 1433–1441. [[CrossRef](#)]
54. Gasquet, D.; Chevremont, P.; Baudin, T.; Chalot-prat, F.; Guerrot, C. Polycyclic Magmatism in the Tagragra d Ō Akka and Kerdous—Tafelast Inliers (Western Anti-Atlas, Morocco). *J. Afr. Earth Sci.* **2004**, *39*, 267–275. [[CrossRef](#)]
55. Pouclet, A.; Ouazzani, H.; Fekkak, A. The Cambrian Volcano-Sedimentary Formations of the Westernmost High Atlas (Morocco): Their Place in the Geodynamic Evolution of the West African Palaeo-Gondwana Northern Margin. *Geol. Soc. London Spec. Publ.* **2008**, *297*, 303–327. [[CrossRef](#)]
56. Oberthur, T.; Melcher, F.; Henjes-Kunst, F.; Gerdes, A.; Stein, H.; Zimmerman, A.; El Ghorfi, M. Hercynian Age of the Cobalt-Nickel-Arsenide-(Gold) Ores, Bou Azzer, Anti-Atlas, Morocco: Re-Os, Sm-Nd, and U-Pb Age Determinations. *Econ. Geol.* **2009**, *104*, 1065–1079. [[CrossRef](#)]
57. Gasquet, D.; Cheilletz, A. L' HydrothermaLisme Un Phénomène CycLique Dans Les Temps GéOLogiques Conséquences Pour La Prospection Minière Au Maroc. *Collect. EDYTEM. Cah. Géographie* **2009**, *9*, 49–56. [[CrossRef](#)]
58. Borisenko, A.S.; Borovikov, A.A.; Pavlova, G.G.; Kalinin, Y.A.; Nevolko, P.A.; Gushchina, L.V.; Lebedev, V.I.; Maacha, L.; Kostin, A.V. Formation Conditions of Hg-Silver Deposition at the Imiter Deposit (Anti-Atlas, Morocco). In *Mineral Deposit Research for a High-Tech World, Proceedings of 12th Biennial SGA Meeting, Uppsala, Sweden, 12–15 August 2013*; Volume 3, pp. 1243–1246.
59. Najih, A.; Montero, P.; Verati, C.; Charaf, M.; Fekkak, A. Initial Pangean Rifting North of the West African Craton: Insights from Late Permian U-Pb and 40 Ar/39 Ar Dating of Alkaline Magmatism from the Eastern Anti-Atlas (Morocco). *J. Geodyn.* **2019**, *132*, 101670. [[CrossRef](#)]
60. Daoud, M.A.; Essalhi, M.; Essalhi, A.; Toummite, A. Petrographic and Magnetic Fabric Investigation of the Tadaout-Tizi n'Rsas Dyke Swarms in the Eastern Anti-Atlas, Morocco. *Econ. Environ. Geol.* **2021**, *54*, 629–647. [[CrossRef](#)]
61. Chamboredon, R. Caractérisation et Origine Des Magmas Alcalins et Des Fluides Sous Le Massif Volcanique Du Jbel Saghro. Ph.D. Thesis, Université de Montpellier, Montpellier, France, 2015.
62. Ikenne, M.; Souhassou, M.; Arai, S.; Soulaïmani, A. A Historical Overview of Moroccan Magmatic Events along Northwest Edge of the West African Craton. *J. Afr. Earth Sci.* **2017**, *127*, 3–15. [[CrossRef](#)]
63. Popov, A.G.; Millar, G.; Belhaj, O.; Sermat, R.; Fettouhi, A. *Gisement Argentifère de Zgounder: Étude Des Minéralisations et Des Roches Encaissantes Porteuses de Sulfures*; Unpubl BRPM Report; Maroc, 1989.

**Disclaimer/Publisher's Note:** The statements, opinions and data contained in all publications are solely those of the individual author(s) and contributor(s) and not of MDPI and/or the editor(s). MDPI and/or the editor(s) disclaim responsibility for any injury to people or property resulting from any ideas, methods, instructions or products referred to in the content.